energies

MDPI

Article

Optimal Design of Thermal Radiative Heating of Horizontal Thin Plates Using the Entropy Generation Minimization Method

Ehsan Gholamalizadeh [1], Mohammad Yaghoub Abdollahzadeh Jamalabadi [2,*] and Majid Oveisi [3]

1 Department of Mechanical Engineering, Sejong University, Seoul 05006, Korea; ehsan@sejong.ac.kr
2 Department of Mechanical, Robotics and Energy Engineering, Dongguk University-Seoul, Seoul 04620, Korea
3 Faculty of Marine Engineering, Chabahar Maritime University, Chabahar 99717-56499, Iran; m.ovisi@cmu.ac.ir
* Correspondence: abdollahzadeh@dongguk.edu or muhammad_yaghoob@yahoo.com; Tel.: +82-10-7435-1362

Received: 26 September 2017; Accepted: 13 November 2017; Published: 21 November 2017

Abstract: Thermal radiant heating through distinct heat sources is of interest for the thermal loading of thin objects as it is used in residential applications, furnaces, and insulator designs. In this paper, an optimal design for a thermal radiant system by discrete suspended heat sources is analyzed in a side open cavity used for heating the top plate, while the bottom plate is kept at a constant temperature, using the entropy generation minimization method. To avoid pressure fluctuations, the semi-implicit method for pressure linked equations method is used, which solves the continuity, Navier-Stokes, fluid energy, and surface energy equations simultaneously. The system is optimized based on the characteristic length of discrete heat sources, height of discrete heat sources from the bottom plate, the distance between discrete heat sources, the number of discrete heat sources, and the aspect ratio of the cavity that finds the optimal location of heating elements. In addition to the geometrical parameters, the effects of the thermal loading parameters on the optimal position are investigated.

Keywords: entropy generation minimization; thermal radiant system; free convection; optimization

1. Introduction

The design of thermal radiative heating of horizontal thin plates is of particular interest in numerous industrial uses as noted by [1–8]. The efficient design of a radiant thermal heating system is interesting to many engineering fields, such as thermal plasma processing [1], metallurgical furnaces [2], hot structure thermal tests [3], coal fired utility boilers [4], thermal loading systems [5], residential heating applications [6–8], etc. Since optimizing the performance of a system to obtain the maximum energy efficiency at the minimum possible economic cost (optimal thermal management) is a worthwhile investigation for those fields. For a typical radiant heating system where the heaters are at the bottom and the object is positioned at the top, the efficiency of the system can be evaluated by the ratio of the heat absorbed (enhanced heat transfer rate) at the top plate and total heat input to the system through the heaters [7]. As well the uniformness of the heat flux received by the top plate, obtaining a specific heat flux profile on the top plate as a vendor request could be another objective function that could be possible through the modification of the system configuration and thermal energy input of the system [6].

The role of discrete heaters and free convection in square and triangular cavities are analyzed with the heat-line concept by Das and Basak [9]. They found an efficient heating strategy based on the

optimal positioning of discrete heaters. As well as this, the effect of different cases based on the heater position in enclosures is studied in [10]. Optimization of discrete heat sources in a vented enclosure is done by Radhakrishnan et al. [11]. Radhakrishnan et al. optimized the problem of discrete staggered heat sources in a vented enclosure numerically and experimentally. They found the coolest heater to maximize heat loading at the minimum temperature deviation by the response surface and trial and error methods. Madadi and Balaji [12] found the optimal location of discrete heat sources with a constant heat flux in a ventilated cavity to minimize the maximum temperature on heat sources using the genetic algorithm method.

Other than optimization based on energy efficiency and thermal management, the designs based on entropy study are explored in the literature. A comprehensive review of entropy generation in natural convection for various enclosure shapes is done by Biswal and Basak [13]. Entropy generation and irreversibility of various fluid types, such as non-Newtonian [14], nano-fluid [15], micro polar fluid [16], Williamson fluid [17], power law fluid [18], etc., is done throughout the literature. The study of entropy generation is a base for entropy generation minimization (EGM) to design a system. Oztop et al. [19] considered the geometrical parameters (opening ratio and center of opening), as well as thermal parameters (Rayleigh number), for optimization. They found that the geometrical parameters are dominant. The effect of obstacles in natural convection is considered by Hussain et al. [20]. It is known that obstacle's position affects the total generated entropy. Moreover, surface thermal radiation can increase the amount of entropy generation by as much as five times [21]. Recently, the entropy generation in the thermal radiative loading of structures with distinct heaters has been studied by Jamalabadi et al. [22]. As shown in most of the cavity (other than zone around the lamps), entropy generation is caused by fluid motion rather than heat transfer. As well as an increase of heating ratio, the heat source number and aspect ratio of irreversibility increases.

Based on the study conducted by Jamalabadi et al. [22], a code was developed using finite volume method with SIMPLE algorithm that solves the governing equation of motion. The code was first validated by comparing the results to those of the benchmark solution from the natural convection of air in a square cavity [23] and also a simulation of a natural convection investigation with a high Rayleigh number in a square cavity [24].

The entropy generation minimization is a type of thermodynamic optimization method, which can be used for optimizing the finite-size systems and finite-time processes [25]. In [25], Bejan demonstrated that the maximum power from a power plant is equivalent to the minimum entropy generation case. This method is consistent with various laws of physics, such as the Bernouli equation (thermodynamics of an inviscid flow) [25], and can be applicable in engineering design problems, such as optimizing a fin length [26], distribution of heat exchanger area [27], intermediate heat transfer of insulation systems [28], optimal heat storage system subject to time constraint [29], extracting maximum power from fluid flow [30], collector design of a solar-thermal power system [31], minimization of heat leak entropy generation for refrigeration systems [32], and several other time dependent processes [33–39].

As shown by the detailed review of optimization based on energy efficiency throughout free convection in enclosures of various shapes, fluids, and processes, the study of the optimal design of free convection in open enclosures with discrete heat sources based on entropy generation minimization has not yet been conducted. The goal of the current research is to optimize the thermal radiative heating of horizontal thin plates by the entropy generation minimization method. This optimization is based on thermal and geometrical parameters with the entropy generation as the objective function.

2. Mathematical Modeling

Open cavity with discrete heat sources considered here is shown in Figure 1. The system studied in the current paper (Cartesian coordinates) consists of a side opened cavity that has thermal interaction with constant temperature sources: the environment (inlet at $T_{in} = T_\infty$ and adiabatic outlet flow) and the bottom plate (solid wall at $T_c = T_\infty$). In accordance with thermal insulator tests and to obtain the highest possible temperature on the top plate, adiabatic conditions are assumed. Discrete heat sources

with known characteristic length (D_L) and constant gap distance (X_L) are suspended at a specific height (h_L) from the bottom plate. The working fluid is compressible and Newtonian. The gravity acts in a downward direction. The summary of equations and boundary conditions are shown in Tables 1 and 2, respectively. Although the three-dimensional (3D) numerical analysis is relatively more accurate when compared to a two-dimensional (2D) one, its computational cost is significantly higher. Hence, due to avoiding a high computational cost and also the simplicity of the problem (less parameters for study), the 2D domain is assumed to simulate the system. Although a 2D analysis neglects the ending effect of heaters and the extension of natural convection cells in the third dimension, this approach is widely used for analyzing a natural convection problem when the length of heaters is comparable to the third direction.

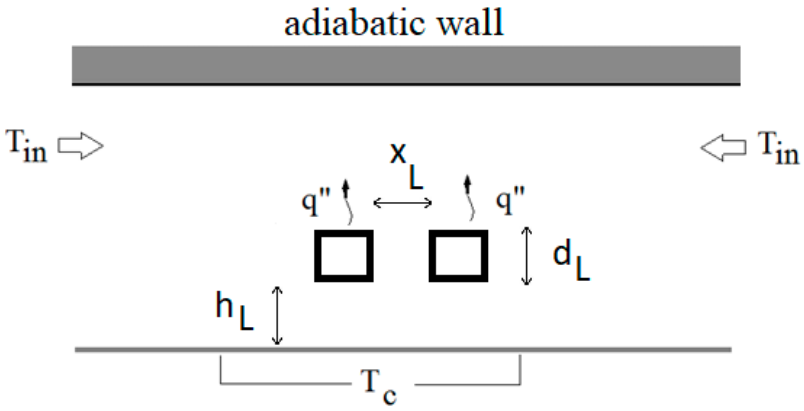

Figure 1. Open cavity with discrete heat sources.

Table 1. Summary of equations.

Equation	Formula
Continuity	$\nabla \cdot \left(\rho \vec{v}\right) = 0$
Equation of State	$P = \frac{8314}{28.97}\rho T$
Momentum	$\left(\vec{v}.\nabla\right)\vec{v} + \frac{\nabla p}{\rho} + g[1 - \alpha(T - T_0)]\,\vec{i}_y = \nu\nabla^2\vec{v}$
Fluid Energy	$\rho c_p\left(\vec{v}.\nabla\right)T = \vec{\vec{\tau}}' : \nabla\vec{v} - \nabla \cdot \vec{q}$
Surface Energy	$\sum\left(\delta_{ij} - F_{ij}\right)\sigma_B T^4 = \sum\left(\delta_{ij} - \left(1 - \varepsilon_j\right)F_{ij}\right)\frac{q''_j}{\varepsilon_j}$

Table 2. Boundary conditions.

Location	Velocity	Temperature
Solid Walls	$\vec{v} = 0$	-
Heat Source Surface	$\vec{v} = 0$	$\frac{\partial T}{\partial n} = \frac{-q''}{k_f}$
Symmetry ($x = 0$)	$u = 0$	$\frac{\partial T}{\partial x} = 0$
Vent ($x = L/2$)	$\frac{1}{2}\rho\vec{v}^2 + p = p_\infty$	$T = T_\infty$

Boundary conditions of solid walls (Table 2) are set as no-slip boundary condition, while a constant heat flux is set to the heat source surfaces. Because of symmetry, a half of the system is modelled to simulate the computational domain (origin of coordinate system is fixed at this line). The temperature gradients that are normal to the symmetric line should be zero, and the horizontal components of

the velocity profile at that place would be zero as well. The vent boundary condition is obtained from Jamalabadi et al. [6]. The unknown values of velocity vector (u, v), pressure, temperature, and density through each point of domain (x, y) could be obtained by solving the continuity equation, Navier–Stokes equations, ideal gas equation of state, fluid energy equation, and solid energy equation where listed in Table 1. The non-dimensional (by k_f/L^2) volumetric rate of irreversibility through the system is given by:

$$\overline{S}_g''' = \left(\frac{L}{T}\right)^2 \left[\left(\frac{\partial T}{\partial x}\right)^2 + \left(\frac{\partial T}{\partial y}\right)^2\right] + \frac{\mu L^2}{T k_f}\left[2\left(\frac{\partial u}{\partial x}\right)^2 + 2\left(\frac{\partial v}{\partial y}\right)^2 + \left(\frac{\partial u}{\partial y} + \frac{\partial v}{\partial x}\right)^2\right] \quad (1)$$

3. Results and Discussion

A code in FORTRAN software (G95, IBM, New York, NY, USA) is developed based on the finite volume method to solve the system of equations. The results of grid dependence tests and comparison with previous works are presented in Tables 3 and 4, respectively.

Table 3. Grid dependence tests at N = 11, A_R = 1 and N_r = 55.31.

ΔX	Max (Ψ)	Relative Error Percent	Nusselt	Relative Error Percent
0.1	285.46	2.3668	53.12	9.5522
0.05	274.93	1.4093	57.37	2.3157
0.01	280.15	0.4626	58.72	0.0170
0.005	278.86	0.0	58.73	0.0

Table 4. Comparison of current study with benchmarks.

Rayleigh	Nusselt		
	De Vahl Davis [23]	Dixit and Babu [24]	This Study
10^3	1.116	1.120	1.13
10^4	2.242	2.286	2.25
10^5	4.531	4.563	4.54
10^6	9.035	8.800	8.9

The optimization results using three lamps with N_r = 1 and A_R = 0.3 are shown in Figure 2. As shown, the generated entropy decreases in direct relation to the increase of the lamp distance from the bottom plate. For the values of h_L that are higher than 0.021, an increase in the lamp distance from the bottom plate causes to increase the irreversibility Therefore, the optimal distance of discrete heat sources is 0.021. The dimensionless quantities of N_r = 10 and A_R = 1/2 are arbitrarily selected to study the effect of the parameters on the system's behavior. The value of the Prandtl number is used here and is adapted with the value of air (Pr = 0.71). An increase in the lamp distance from the bottom plate causes a decrease in the entropy generation due to the heat transfer as a result of a decrease in temperature gradients. When the distance of the heat sources from the bottom plate increases, the action region of heat sources at the cooling plate increases, which leads to a decrease in the temperature gradients. At the same time, an increase in the lamp distance from the bottom plate causes an increase in the entropy generation due to the friction as a result of an increase in the natural convection force. The increase of distance of the heat sources from the bottom plate also lets a higher space of the natural convection. Consequently, since the length of the path that fluid gains energy increases, the velocity increases. It then causes higher amount of vorticity generated entropy.

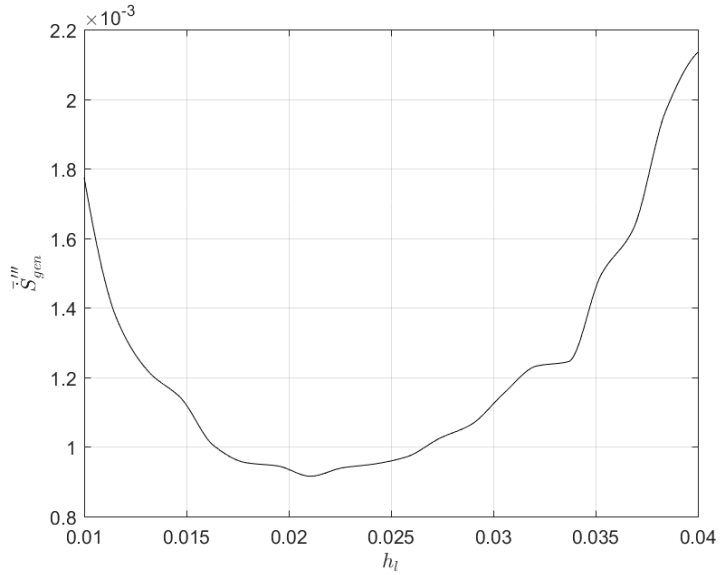

Figure 2. Generated entropy vs. the lamp distance from the bottom plate for $N_r = 10$ and $A_R = 1/2$.

The one parameter optimization of the system is done around the condition of $N = 13$ (Number of heat sources), $A_R = 0.3$ (aspect ratio is defined by height to length ratio of the cavity), $N_r = 1$ (heating number = $q''/\sigma T_\infty{}^4$), $D_L = 0.01$ (the ratio of heat source characteristic length to length of the cavity), $h_L = 0.02$ (the ratio of the height of heat sources from the bottom plate), and $x_L = 0.02$ (the ratio of the gap between the heat sources to length ratio of the cavity) as shown in Figures 3–6.

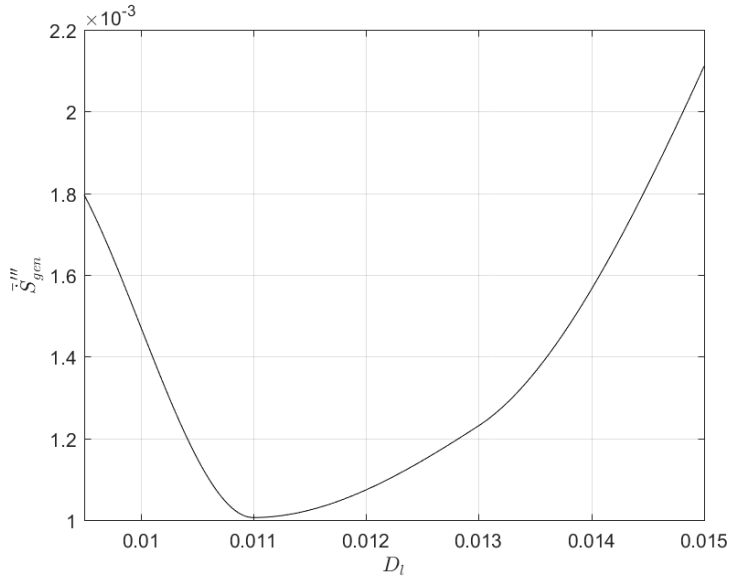

Figure 3. Generated entropy vs. the lamp diameter for $N_r = 10$ and $A_R = 1/2$.

Figure 3 depicts that, for $N_r = 10$ and $A_R = 1/2$, the generated entropy decreases when the lamp diameter is increased. As shown in this figure, the optimal diameter of discrete heat sources is equal to $D_L = 0.011$. When the lamp diameter increases, an increase in the lamp perimeter causes a decrease in the surface temperature, which results in a decrease in the heat component of irreversibility production. In addition, at a constant distance between lamps, an increase in the lamp diameter causes an increase in the surface of heat transfer while it intensifies the fluid flow inspired by natural convection motion.

The confrontation of these two effects meets at the point of D_L = 0.011 for current study. Figure 4 shows that, for N_r = 10, an increase in the aspect ratio causes to decrease the generated entropy. It can be observed that, in the range of 0.29 < A_R < 0.36, the irreversibility reaches its minimum value. When the aspect ratio increases, the entropy generation due to the heat transfer decreases as a result of a decrease in the temperature gradients. Moreover, the distance between two heat sources and heat sink in the system increases, which results in a decrease in the temperature gradients. An increase in the aspect ratio also causes an increase in the entropy generation due to the friction as a result of an increase in the natural convection force. A higher aspect ratio causes a larger size of natural convection. Since the distance of the path that fluid obtains energy increases, the velocity increase. Consequently, it results in a higher amount of vorticity generated entropy.

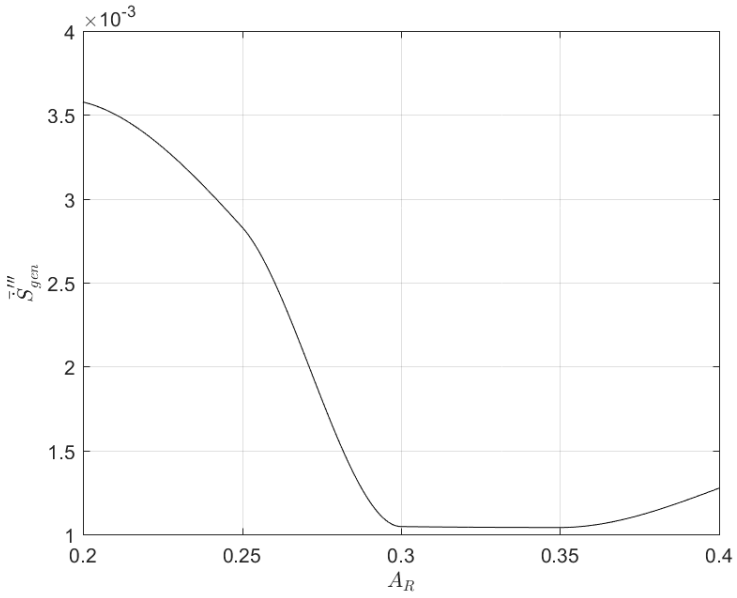

Figure 4. Generated entropy vs. the aspect ratio for N_r = 10.

The generated entropy as a function of the gap between lamps for N_r = 10 and A_R = 1/2 is plotted in Figure 5. It is clear that x_L = 0.02 is the optimal location of the heaters. As the gap between lamps increase, the total distance of the region of the heat sources increases. This causes both components of the entropy production to decrease until the total length of the region is extended to near the natural convection cell at the outlet of the system. At that point, the entropy production due to the friction demolishes suddenly, which causes an increase in the entropy generation. The confrontation of these two effects meets at the point x_L = 0.02 in this study.

The generated entropy as a function of the lamp number for N_r = 6 and A_R = 0.3 is plotted in Figure 6. It can be observed that an increase in the heat source number causes an increase in the irreversibility constantly. Therefore, the optimal number for the heaters is one heater. An increase in the heat source numbers causes an increase for both components of the entropy productions, including the friction and the heat transfer, which produce irreversibility through the system. Hence, it is found that using less heat sources is efficient based on the second law analysis.

Figure 7 shows the distribution of the dimensionless total rate of entropy generation (by k_f/L^2) for three discrete heat sources with N_r = 1 and A_R = 1/2. For this configuration and input heat flux, most of the irreversibility is produced at the open side of the cavity. The zone near the lamps where the highest temperature gradient occurred does not contain the highest entropy generation, while the open side that contains the highest magnitude of vortex generation has the highest values of irreversibility and most energy quality is lost at that zone. The maximum entropy generation rate occurred at the inlet of air near the heated top wall.

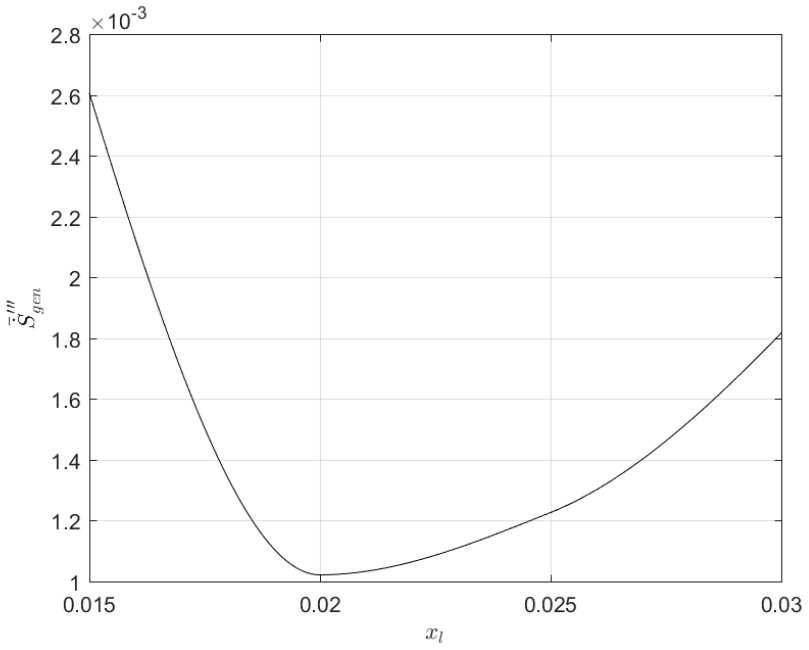

Figure 5. Generated entropy vs. the gap between lamps for $N_r = 10$ and $A_R = 1/2$.

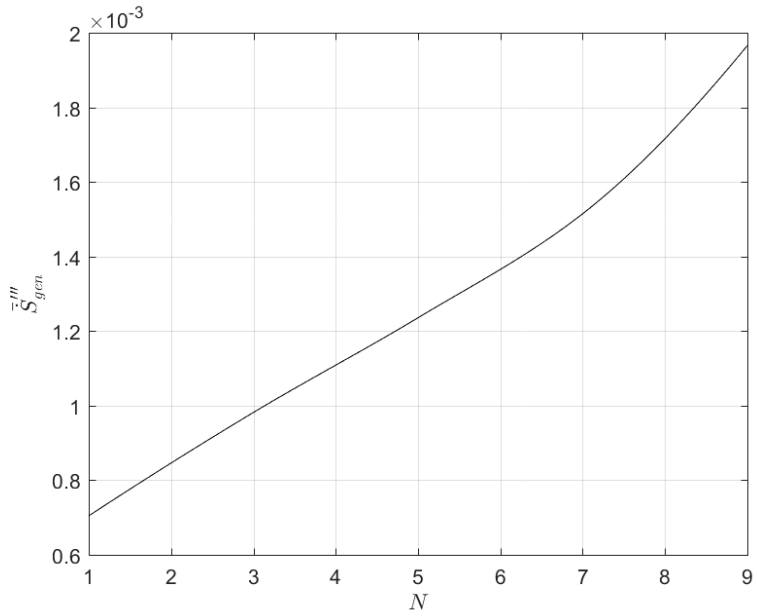

Figure 6. Generated entropy vs. the lamp number for $N_r = 10$ and $A_R = 1/2$.

The contribution of various parts of entropy generation is clearly expressed by Figure 8. The ratio of heat transfer contribution in terms of total entropy generation is defined by the Bejan number. Figure 8 shows the contours of the Bejan number for $N = 13$, $N_r = 1$, and $A_R = 0.3$, and it is obvious that the dominant heat transfer zone is restricted to near the discrete heat sources and extends to the heated top plate. The rest of the cavity has a Bejan number of less than the value of 0.05. It means that more than 95 percent of the entropy is generated by fluid friction. That viscous heating is aroused by natural convection through the cavity.

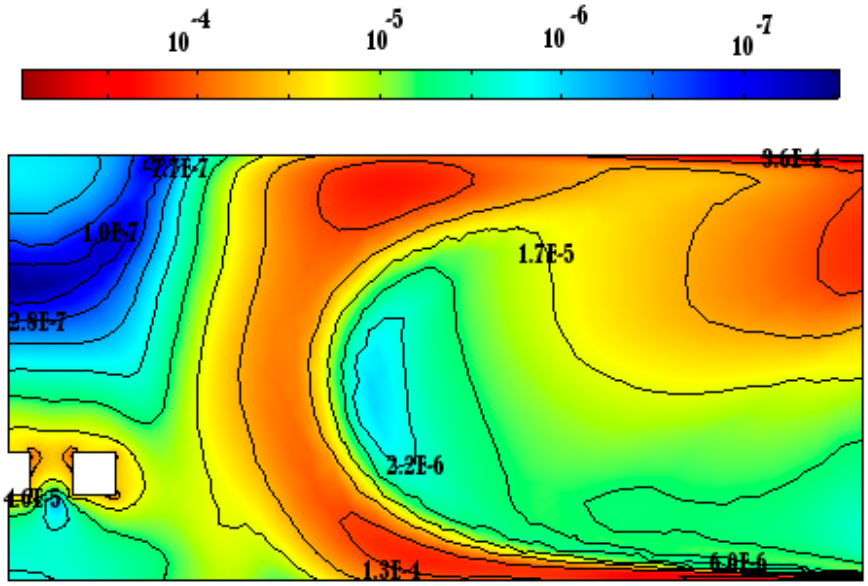

Figure 7. Dimensionless rate of total entropy generation for $N = 3$, $N_r = 1$, and $A_R = 1/2$.

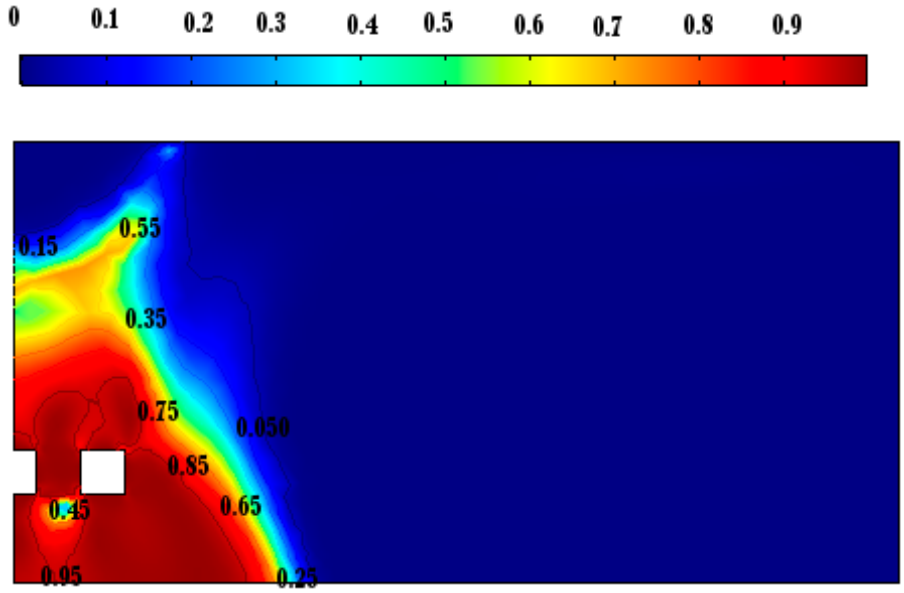

Figure 8. Bejan number for $N = 3$, $N_r = 1$, and $A_R = 1/2$.

Other than the one parameter optimization done in Figures 3–6, in many applications it is necessary to optimize the system parameters together. Figure 9 reveals the variation of dimensionless total entropy generation rate per unit volume (k_f/L^2) throughout the open cavity for $N = 13$ and $N_r = 1$ as a function of the aspect ratio and the height of discrete heat sources from the bottom. The 2D profile of that 3D surface is plotted in Figure 10 to make its values clear. As shown, based on the value of the aspect ratio, there are different optimums in the range that is used for the height of discrete heat sources from the bottom. The saddle shape surface shown in Figure 10 has a dent near the surface of $A_R = 0.3$. The point $h_L = 0.02$ is the optimum point for $A_R = 0.31$, but it is the worst choice when $A_R = 0.65$. Hence, the recommended values should be used in the specified condition and could not be used in all of the ranges.

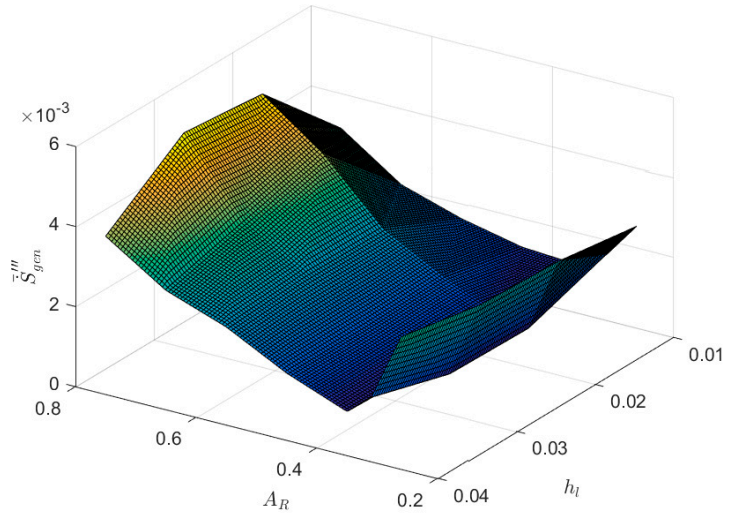

Figure 9. Dimensionless rate of total entropy generation for N = 13, and N_r = 1 as a function of aspect ratio and the height of discrete heat sources from the bottom.

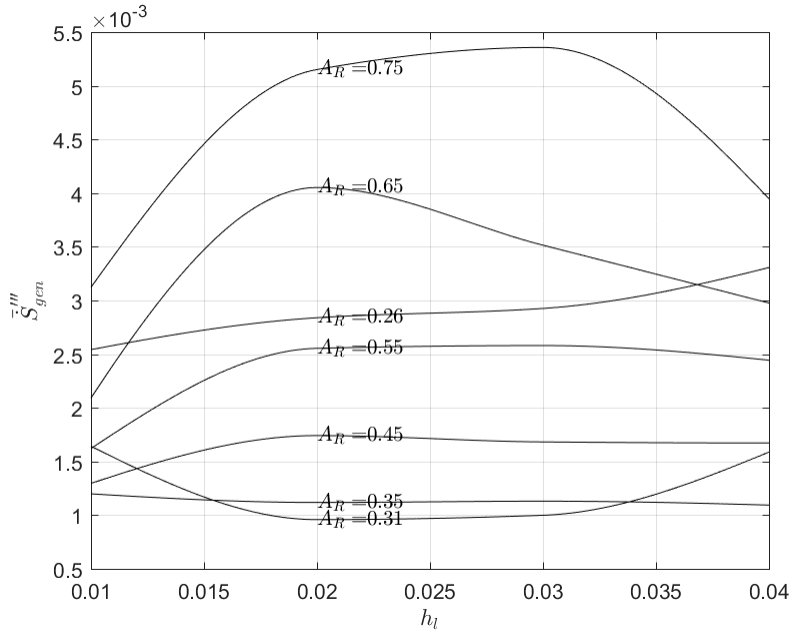

Figure 10. Dimensionless rate of total entropy generation for N = 13, and N_r = 1 as a function of the height of discrete heat sources from the bottom for various aspect ratios.

It was also shown in [22] that the total entropy generation rate per volume throughout the open cavity is increased for N_r higher than one (for lower values where the heat conduction is dominant, it is almost constant), but these conditions are not true in all of the cases. Proof of this is plotted in Figure 11, which demonstrates the role of heat source number and heating ratio in entropy generation, while the total rate of entropy generation per volume surface is schemed against the heating ratio for various numbers of heat sources in the open cavity. As shown for the values of heat source number over 15, entropy generation suddenly decreases. That happens because in those conditions most of the cavity space is filled by heat sources. Therefore, the zone near the open side is restricted by heat sources which produces the highest amount of irreversibility (due to fluid friction). Hence, the greatest contribution of the generated entropy would be based on the thermal radiation heat transfer mode and the natural convection heat transfer mode.

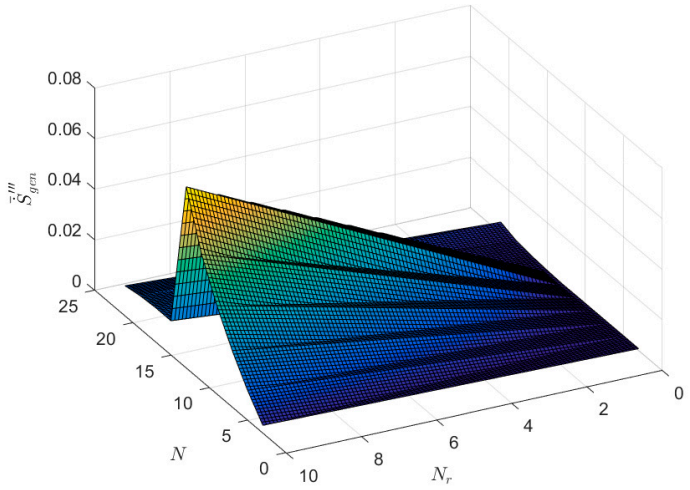

Figure 11. Dimensionless rate of total entropy generation as a function of heat source number and the heating ratio.

4. Conclusions

The results of our comprehensive investigation on thermal radiant heating by distinct heat sources on the thermal loading of thin objects were presented. The schemed problem is used in residential applications, furnaces, and insulator designs. In this research, the optimal design of a thermal radiant system by discrete suspended heat sources in a side open cavity is used to heat the top plate while the bottom plate is kept at a constant temperature was performed via the entropy generation minimization method. The SIMPLE method is used to solve the continuity, Navier-Stokes, fluid energy, and surface energy equations, simultaneously. The optimization of the system is done around the condition of $N = 13$, $A_R = 0.3$, $N_r = 1$, $D_L = 0.01$, $h_L = 0.02$, and $x_L = 0.02$. Optimization was performed based on the characteristic length of discrete heat sources, height of discrete heat sources from the bottom plate, distance between discrete heat sources, number of discrete heat sources, and aspect ratio of the cavity to find the optimal location of heating elements. As well as geometrical parameters, thermal loading parameters effects are investigated for optimal positions. These limitations should be considered in practical applications of the method and results of this paper. The results are summarized as follows:

(1) In the range of 0.29 to 0.36 the aspect ratio has minimum irreversibility.
(2) The optimal gap between the heat sources is 0.02 of the length of the cavity.
(3) The optimal height of the heat sources from the bottom plate is 0.02 of the length of the cavity at an aspect ratio of 0.3.
(4) The optimal characteristic size of heat sources is 0.011 of the length of the cavity.
(5) By increasing the number of heat sources entropy generation increases. The optimal value occurs in one heater.
(6) The maximum entropy generation rate occurred at the inlet of air near the heated top wall.
(7) The dominant heat transfer zone is restricted to near discrete heat sources and extends to the heated top plate. The rest of the cavity has a Bejan number of less than the value of 0.05.
(8) The point $h_L = 0.02$ results in the minimum entropy generation when $A_R = 0.31$. It also results in the maximum entropy generation when $A_R = 0.65$. Hence, the recommended values cannot be used in all of the ranges, but is applicable in a specific condition.
(9) For the values of heat source number over 15, the natural convection zone is choked by the presence of heat sources and entropy generation suddenly decreases.

Acknowledgments: This work was supported by the faculty research fund of Sejong University in 2017.

Author Contributions: Conceptualization, analysis, investigation, methodology, software, validation, visualization, writing the original draft, and editing were done by M.Y.A.J. E.G. supported the research and grammatically reviewed the manuscript. Research resource was also partially provided by M.O. and M.Y.A.J. All authors have read and approved the final manuscript.

Conflicts of Interest: The authors declare no conflict of interest.

Nomenclature

A_R	*Aspect ratio (H/L)*
Be	*Bejan number*
Br	*Brinkmann number*
Cp	*specific heat at constant pressure* ($J \cdot K^{-1}$)
Gr	*Grashof number* ($g\beta L^4 q''/\nu^2$)
F_{ij}	*Configuration factor*
F_b	*body force*
g	*acceleration due to gravity* ($m \cdot s^{-2}$)
H	*Enclosure height* (m)
k	*thermal conductivity* ($W \cdot m^{-1} \cdot K^{-1}$)
L	*characteristic length* (m)
n	*number of heat sources*
N_r	heating number ($q''/\sigma T_\infty{}^4$)
N_s	entropy generation number
Nu	*local Nusselt number*
p	*pressure* (Pa)
P	*dimensionless pressure* ($(p\text{-}p_\infty)L^2/\rho\alpha^2$)
Pr	*Prandtl number (ν/α)*
q''	*Heater heat flux* ($W \cdot m^{-2}$)
Ra	Rayleigh number ($g\beta L^4 q''/\nu\alpha$)
Re	Reynolds number
S'''	entropy generation rate per volume
S	dimensionless entropy generation
S_θ	dimensionless local entropy generation due to heat transport
S_ψ	dimensionless local entropy generation due to fluid friction
S_θ, *total*	dimensionless total entropy generation due to heat transport
S_ψ, *total*	dimensionless total entropy generation due to fluid friction
Stotal	dimensionless total entropy generation due to heat and fluid friction
T	temperature of the fluid (K)
Th	temperature of hot wall (K)
Tc	temperature of cold wall (K)
U	*x* component of dimensionless velocity (v_x *L*/α)
V	*y* component of dimensionless velocity (v_y *L*/α)
v	velocity vector
v_x	*x* component of velocity ($m \cdot s^{-1}$)
v_y	*y* component of velocity ($m \cdot s^{-1}$)
x	distance along *x* coordinate (m)
X	dimensionless distance along *x* coordinate (*x*/*H*)
y	distance along *y* coordinate (m)
Y	dimensionless distance along *y* coordinate (*y*/*H*)

Greek Symbols

α	thermal diffusivity ($m^2 \cdot s^{-1}$)
β	volume expansion coefficient (K^{-1})
δ_{ij}	Kronecker delta
ϵ	surface emission factor
θ	dimensionless temperature
μ	dynamic viscosity ($kg \cdot m^{-1} \cdot s^{-1}$)
ρ	density ($kg \cdot m^{-3}$)
ζ	dimensionless heat flux ($q''/\sigma T_\infty{}^4$)
Φ	viscous dissipation functions
ϕ	irreversibility distribution ratio
ψ_d	dimensional streamfunction ($m^2 \cdot s^{-1}$)
ψ	dimensionless streamfunction

Subscripts

∞	bulk, ambient value
m	mean, modified, spatial average
f	fluid
eff	effective properties of fluid
s	solid
$total$	summation over the domain

Superscripts

e	element

References

1. Bertrand, P.; Ignatiev, M.; Flamant, G.; Smurov, I. Pyrometry applications in thermal plasma processing. *Vacuum* **2000**, *56*, 71–76. [CrossRef]
2. Ertem, M.E.; Sen, S.; Akar, G.; Pamukcu, C.; Gurgen, S. Energy balance analysis and energy saving opportunities for Erdemir slab furnace. *Energy Sources Part A Recovery Util. Environ. Eff.* **2010**, *32*, 979–994. [CrossRef]
3. Jamalabadi, M.Y.A. Experimental investigation of thermal loading of a horizontal thin plate using infrared camera. *J. King Saud Univ. Eng. Sci.* **2014**, *26*, 159–167.
4. Shimoda, H.; Sugano, A.; Watanabe, Y.; Kimura, T.; Ishiyama, K. Prediction method of unburnt carbon for coal fired utility boiler using image processing technique of combustion flame. *IEEE Trans. Energy Convers.* **1990**, *5*, 640–645. [CrossRef]
5. Jamalabadi, M.Y.A.; Ghassemi, M.; Hamedi, M.H. Two-dimensional simulation of thermal loading with horizontal heat sources. *Proc. Inst. Mech. Eng. Part C J. Mech. Eng. Sci.* **2012**, *226*, 1302–1308. [CrossRef]
6. Abdollahzadeh Jamalabadi, M.Y.; Ghassemi, M.; Hamedi, M.H. Numerical investigation of thermal radiation effects on open cavity with discrete heat sources. *Int. J. Numer. Methods Heat Fluid Flow* **2013**, *23*, 649–661. [CrossRef]
7. Jamalabadi, M.Y.A. Effect of temperature dependent properties on thermal radiative loading of planar surfaces with distinct heaters. *J. Niger. Math. Soc.* **2016**, *35*, 159–177. [CrossRef]
8. Woodson, R. *Radiant Floor Heating*; McGraw-Hill: New York, NY, USA, 2010; ISBN 978-0-07-159936-8.
9. Das, D.; Basak, T. Role of distributed/discrete solar heaters for the entropy generation studies in the square and triangular cavities during natural convection. *Appl. Therm. Eng.* **2017**, *113*, 1514–1535. [CrossRef]
10. Doo, J.H.; Mun, G.S.; Ha, M.Y.; Seong, S.Y. Thermodynamic irreversibility induced by natural convection in square enclosure with inner cylinder. Part-II: Effect of vertical position of inner cylinder. *Int. J. Heat Mass Transf.* **2016**, *97*, 1120–1139. [CrossRef]
11. Radhakrishnan, T.V.; Balaji, C.; Venkateshan, S.P. Optimization of multiple heaters in a vented enclosure—A combined numerical and experimental study. *Int. J. Therm. Sci.* **2010**, *49*, 721–732. [CrossRef]

12. Madadi, R.R.; Balaji, C. Optimization of the location of multiple discrete heat sources in a ventilated cavity using artificial neural networks and micro genetic algorithm. *Int. J. Heat Mass Transf.* **2008**, *51*, 2299–2312. [CrossRef]
13. Biswal, P.; Basak, T. Entropy generation vs energy efficiency for natural convection based energy flow in enclosures and various applications: A review. *Renew. Sustain. Energy Rev.* **2017**, *80*, 1412–1457. [CrossRef]
14. Kefayati, G.H.R. Heat transfer and entropy generation of natural convection on non-Newtonian nanofluids in a porous cavity. *Powder Technol.* **2016**, *299*, 127–149. [CrossRef]
15. Sheremet, M.A.; Oztop, H.F.; Pop, I.; Abu-Hamdeh, N. Analysis of entropy generation in natural convection of nanofluid inside a square cavity having hot solid block: Tiwari and Das' model. *Entropy* **2016**, *18*, 9. [CrossRef]
16. Abdollahzadeh Jamalabadi, M.Y. Entropy generation in boundary layer flow of a micro polar fluid over a stretching sheet embedded in a highly absorbing medium. *Front. Heat Mass Transf.* **2015**, *6*, 1–13. [CrossRef]
17. Abdollahzadeh Jamalabadi, M.Y.; Hooshmand, P.; Bagheri, N.; KhakRah, H.; Dousti, M. Numerical Simulation of Williamson Combined Natural and Forced Convective Fluid Flow between Parallel Vertical Walls with Slip Effects and Radiative Heat Transfer in a Porous Medium. *Entropy* **2016**, *18*, 147. [CrossRef]
18. Hooshmand, P.; Gatabi, H.R.; Bagheri, N.; Pirzadeh, I.; Hesabi, A.; Abdollahzadeh Jamalabadi, M.Y.; Oveisi, M. Numerical Study of the Magnetic Field Effects on the Heat Transfer and Entropy Generation Aspects of a Power Law Fluid over an Axisymmetric Stretching Plate Structure. *Entropy* **2017**, *19*, 94. [CrossRef]
19. Oztop, H.F.; Kolsi, L.; Alghamdi, A.; Abu-Hamdeh, N.; Borjini, M.; Aissia, H.B. Numerical analysis of entropy generation due to natural convection in three-dimensional partially open enclosures. *J. Taiwan Inst. Chem. Eng.* **2017**, *75*, 131–140. [CrossRef]
20. Hussain, S.; Ahmed, S.E.; Akbar, T. Entropy generation analysis in MHD mixed convection of hybrid nanofluid in an open cavity with a horizontal channel containing an adiabatic obstacle. *Int. J. Heat Mass Transf.* **2017**, *114*, 1054–1066. [CrossRef]
21. Hinojosa, J.F.; David, B.; Xamán, J.; Pérez-Tello, M. The effect of surface thermal radiation on entropy generation in an open cavity with natural convection. *Int. Commun. Heat Mass Transf.* **2017**, *81*, 164–174. [CrossRef]
22. Abdollahzadeh Jamalabadi, M.Y.; Safaei, M.R.; Alrashed, A.A.A.A.; Nguyen, T.K.; Bandarra Filho, E.P. Entropy Generation in Thermal Radiative Loading of Structures with Distinct Heaters. *Entropy* **2017**, *19*, 506. [CrossRef]
23. Vahl Davis, D.G. Natural convection of air in a square cavity: A benchmark solution. *Int. J. Numer. Methods Fluids* **1983**, *3*, 249–264. [CrossRef]
24. Dixit, H.N.; Babu, V. Simulation of high Rayleigh number natural convection in a square cavity using the lattice Boltzmann method. *Int. J. Heat Mass Transf.* **2006**, *49*, 727–739. [CrossRef]
25. Bejan, A. *Entropy Generation Minimization: The Method of Thermodynamic Optimization of Finite-Size Systems and Finite-Time Processes*; CRC Press: New York, NY, USA, 1996.
26. Poulikakos, D.; Bejan, A. Fin Geometry for Minimum Entropy Generation in Forced Convection. *J. Heat Transf.* **1982**, *104*, 616–623. [CrossRef]
27. Guo, J.; Cheng, L.; Xu, M. Optimization design of shell-and-tube heat exchanger by entropy generation minimization and genetic algorithm. *Appl. Therm. Eng.* **2009**, *29*, 2954–2960. [CrossRef]
28. Bejan, A. A general variational principle for thermal insulation system design. *Int. J. Heat Mass Transf.* **1979**, *22*, 219–228. [CrossRef]
29. Andresen, B.; Gordon, J.M. Optimal paths for minimizing entropy generation in a common class of finite-time heating and cooling processes. *Int. J. Heat Fluid Flow* **1992**, *13*, 294–299. [CrossRef]
30. Bejan, A. Maximum power from fluid flow. *Int. J. Heat Mass Transf.* **1996**, *39*, 1175–1181. [CrossRef]
31. Kalogirou, A. Solar thermal collectors and applications, Solar thermal collectors and applications. *Prog. Energy Combust. Sci.* **2004**, *30*, 231–295. [CrossRef]
32. Ratts, E.B.; Brown, J.S. A generalized analysis for cascading single fluid vapor compression refrigeration cycles using an entropy generation minimization method. *Int. J. Refrig.* **2000**, *23*, 353–365. [CrossRef]
33. Hasani, R.; Jafarzadeh, H.; Khoshalhan, F. A new method for supply chain coordination with credit option contract and customers' backordered demand. *Uncertain Supply Chain Manag.* **2013**, *1*, 207–218. [CrossRef]

34. Jafarzadeh, H.; Gholami, S.; Bashirzadeh, R. A new effective algorithm for on-line robot motion planning. *Decis. Sci. Lett.* **2014**, *3*, 121–130. [CrossRef]
35. Moradinasab, N.; Amin-Naseri, M.R.; Behbahani, T.J.; Jafarzadeh, H. Competition and cooperation between supply chains in multi-objective petroleum green supply chain: A game theoretic approach. *J. Clean. Prod.* **2018**, *170*, 818–841. [CrossRef]
36. Jafarzadeh, H.; Moradinasab, N.; Gerami, A. Solving No-Wait Two-Stage Flexible Flow Shop Scheduling Problem with Unrelated Parallel Machines and Rework Time by the Adjusted Discrete Multi Objective Invasive Weed Optimization and Fuzzy Dominance Approach. *J. Ind. Eng. Manag.* **2017**, *10*, 73–89. [CrossRef]
37. Elyasi, M.; Jafarzadeh, H.; Khoshalhan, F. An Economical order Quantity Model for Items with Imperfect Quality: A Non-Cooperative Dynamic Game Theoretical Model. Available online: http://en.seminars.sid.ir/ViewPaper.aspx?FID=464e20160508 (accessed on 21 November 2017).
38. Elyasi, M.; Jafarzadeh, H.; Khoshalhan, F. Hybrid Ant Colony Optimization (ACO) algorithm for no-wait flow-shop makespan. In Proceedings of the 5th International Conference of the Iranian Society of Operations Research, Tabriz, Iran, 16–17 May 2012; pp. 16–17.
39. Jafarzadeh, H.; Moradinasab, N.; Eskandari, H.; Gholami, S. Genetic Algorithm for a Generic Model of Reverse Logistics Network. *Int. J. Eng. Innov. Res.* **2017**, *6*, 174–178.